AIAA 81-4074

# Correlation of Artificially Induced Boundary-Layer Transition Data at Hypersonic Speeds

A. H. Boudreau*
*Sverdrup/ARO, Inc., Arnold Air Force Station, Tenn.*

**Previous investigations of distributed-roughness boundary-layer trips indicated that they are superior to spherical-type trips in that equally effective distributed-roughness trips are one-fifth as high and produce substantially smaller flowfield disturbances. The present work has expanded the data base, permitting correlation of distributed-roughness tripping data. The correlation thus developed includes a wide range of Reynolds numbers, cone angles, and trip heights. Plots are provided that permit the selection of distributed-roughness trips without the need of boundary-layer solutions.**

## Nomenclature

$k$ = trip element height, in.
$M_\infty$ = freestream Mach number
$P_E$ = pressure at the end of the roughness area ($s/r_n = 5$), psia
$P_0'$ = freestream pitot pressure, psia
$p_\infty$ = freestream pressure, psia
$q_\infty$ = freestream dynamic pressure, psia
$Re_{e,\theta}$ = Reynolds number based on boundary-layer edge conditions and momentum thickness
$Re_{e,r_n}$ = Reynolds number based on boundary-layer edge conditions and model nose radius
$Re_\infty$/ft = Reynolds number based on freestream conditions and a 1 ft length
$Re_{\infty,r_n}$ = Reynolds number based on freestream conditions and model nose radius
$r_b$ = model base radius, in.
$r_n$ = model nose radius, in.
$s$ = surface distance along the model measured from the stagnation point, in.
$T_e$ = temperature at the edge of the boundary layer, °R
$T_{0_\infty}$ = freestream total temperature, °R
$T_w$ = model wall temperature, °R
$T_\infty$ = freestream temperature, °R
$X$ = Mayne's correlation parameter, see Eq. (3)
$\theta$ = boundary-layer momentum thickness, in.
$\theta_c$ = model cone half-angle, deg
$\lambda$ = PANT correlation parameter, see Eq. (1)
$\lambda_M^*$ = modified PANT correlation parameter evaluated at the sonic point, see Eq. (5)

*Subscripts*

critical = value of the parameter needed to bring transition up to or near the trip
$t$ = at the end of transition

*Superscript*

* = evaluated at the sonic point

## Introduction

PREVIOUS work[1] examined the field of roughness-induced transition and explored various correlation techniques. In addition, limited tests were performed to find an optimum tripping device. These tests indicated the clear advantage of using distributed-roughness-type trips instead of the commonly employed spherical trips. Distributed-roughness trips were one-fifth as large as spherical trips yet provided the same trip effectiveness, thus implying significantly less flowfield disturbance. The previous tests were limited, however, to a 7 deg blunt cone tested over a very limited Reynolds number range. Thus, the data base was insufficient to develop a meaningful correlation.

The present work has been directed toward expanding the data base and developing a prediction technique. A primary objective in developing this correlation was to make its use independent of further boundary-layer solutions. Hence, plots have been developed (Appendix A) that allow the reader to size trips using only the information in this paper.

Submitted April 18, 1980; revision received Sept. 12, 1980.


*Senior Project Engineer, von Kármán Gas Dynamics Facility, AEDC Division.

## Experimental Apparatus

### AEDC-VKF Tunnel F

Tunnel F is an arc-driven wind tunnel of the hotshot type,[2,3] and capable of providing Mach numbers of about 7-13 over a Reynolds number per foot range of $0.20\text{-}50 \times 10^6$.

This test was conducted using the 40 in. exit diam contoured nozzle in the 54 in. diam test section to obtain a nominal freestream Mach number of 9.0. Nitrogen was the test gas. Because of the relatively short (100 ms) test times, the model wall temperature remained essentially invariant from the initial value of approximately 540 °R; thus $T_w/T_{0_\infty} \cong 0.15\text{-}0.35$, which approximates the condition of practical interest for re-entry vehicles.

### Models

Models used in the present investigation consisted of an $r_n = 0.5$ in., 5 deg, half-angle cone and an $r_n = 0.589$ in., 7 deg, half-angle cone with an alternate 14 deg biconic nose section. These models are shown in Figs. 1-3, respectively. The primary instrumentation on these models was coaxial heat-transfer gages. The trips used were identical to those used in the previous tests[1] and are described in Table 1.

### Instrumentation

Coaxial surface thermocouple gages were used to measure the surface heating-rate distributions. In practical measurement applications, the surface thermocouple behaves as a homogeneous, one-dimensional, semi-infinite solid. The instrument provides an electromotive force (emf) directly proportional to surface temperature that may be related by theory to the incident heat flux. All heat-transfer gages were

**Table 1 Trip descriptions**

| Type of trip | Description |
|---|---|
| Grit blast | Surface roughness was produced by impacting hardened steel particles onto the stainless-steel nose. RMS peak-to-valley roughness height was 5 mils. Roughness was $s/r_n = 0$-5, determined by photomicrographs of samples. |
| Numerically controlled machine (NCM) | Roughness elements were machined as pyramids with a total height (peak-to-valley) of 8 and 14 mils. The base plane of the pyramids was recessed one-third of the height below the original unaltered model surface. The roughness was $s/r_n = 0.1$-5, measured on optical comparators. |
| Grit | Roughness elements consisted of silicon carbide grit particles bonded to the model surface with epoxy. Grit sizes of 10, 14, 20, 36, and 40 mils were used, and coverage was $s/r_n = 0.8$-5. Roughness was defined by using Fig. A3, Appendix A. |
| 0.063 and 0.109 in. spheres (7 deg model) | Tripping elements consisted of two rows of spheres: a row of 0.063 in. spheres at $s/r_n = 3.1$ and a row of 0.109 in. spheres at $s/r_n = 6.5$. Lateral spacing was four diameters. The spheres were spot welded to thin metal bands that were then bonded to the model. |
| 0.039 in. spheres (14 and 7 deg biconic) | Tripping elements consisted of a single row of 0.039 in. spheres at $s/r_n = 6.8$. The spheres were laterally spaced four diameters apart and spot welded to thin metal bands that were then bonded to the model surface. |

**Table 2 Test conditions**

| $M_\infty$ | $Re_\infty$/ft $\times 10^{-6}$ | $p_\infty$, psia | $T_\infty$, °R | $q_\infty$, psia |
|---|---|---|---|---|
| 9.0 | 20.0 | 0.46 | 102 | 25.5 |
| | 18.0 | 0.43 | 107 | 24.5 |
| | 14.0 | 0.38 | 117 | 21.0 |
| 8.5 | 10.0 | 0.28 | 111 | 13.9 |
| | 8.0 | 0.25 | 123 | 13.0 |
| | 5.0 | 0.20 | 143 | 10.0 |
| 8.7 | 3.0 | 0.12 | 152 | 6.9 |
| 8.0 | 2.0 | 0.09 | 166 | 5.2 |

bench calibrated before installation into the model. The precision of these calibrations is estimated to be ±3%.

## Procedures

### Test Conditions

Test conditions for the 40 in. nozzle of Tunnel F are shown in Table 2. Conditions vary from run to run in Tunnel F, and the values listed are nominal values.

### Test Procedures

The present tests complement previous work[1] in AEDC-VKF Tunnels B and F. The primary variables of Reynolds number, cone angle, and trip height were expanded in the current tests to promote a broad data base for correlation. Reynolds number was varied 0.5-20.5 $\times 10^6$/ft, cone angle 5-14 deg, and trip height 5-40 mils. Angle of attack was maintained at zero, and model wall temperature ratio ($T_w/T_{0_\infty}$) remained relatively constant at 0.15-0.35. A listing

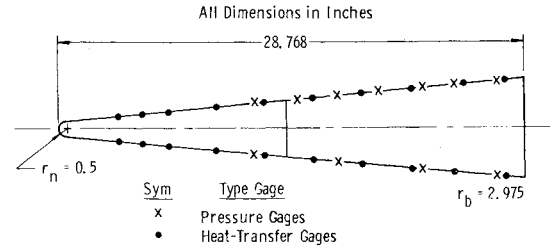


**Fig. 1 Five-degree cone model.**

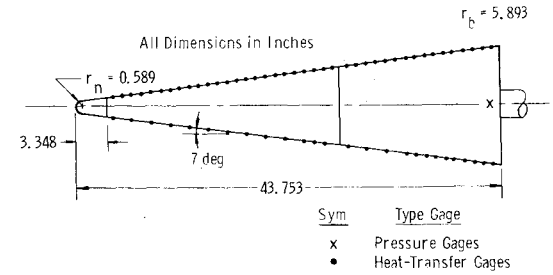


**Fig. 2 Large-pressure heat-transfer model (7 deg cone).**

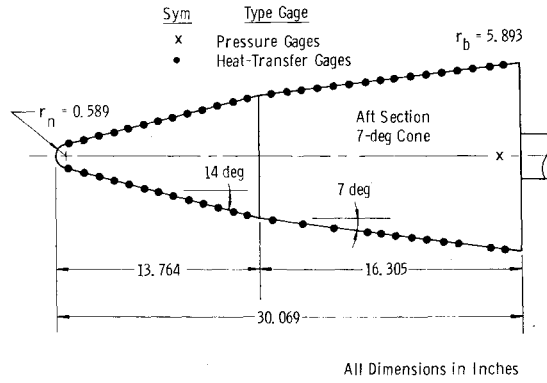


**Fig. 3 The 14–7-deg biconic model.**

of primary variables is included in Appendix B along with a complete tabulation of the current test results.

As discussed in the previous work,[1] the point at which fully turbulent flow is established is defined as that point at which the heat-transfer rate reaches a peak or levels off to agree with turbulent theory.

## Data Precision

For the Tunnel F tests, the uncertainties in measured data account for dynamics of the measurements and system errors. Representative values are: $M_\infty = 3\%$, $p_\infty = 7\%$, $T_\infty = 8\%$, and $Re_\infty/\text{ft} = 11\%$.

## Correlation of Results

In recent years, a great deal of interest has been generated in the area of roughness-induced transition on re-entry vehicles. The commonly termed "PANT correlation" has become an accepted standard in the design of re-entry nosetips where roughness is present. Anderson[4] has shown that by using $Re_{e,\theta}$ as an amplification parameter and the expression $(T_e/T_w)(k/\theta)$ as a modified relative roughness, a PANT correlation is derived that can predict the onset and location of transition on a roughened nosetip. The equation thus arrived at is

$$\lambda = Re_{e,\theta}\left(\frac{T_e}{T_w}\frac{k}{\theta}\right)^{0.7} = 255 \text{ required at sonic point for transition} \quad (1)$$

A.W. Mayne,[5] has formulated a parameter $X$ independent of Reynolds number which makes the boundary-layer solutions necessary to apply the correlation a function of only $M_\infty$ and $T_w/T_{0_\infty}$. Laminar boundary-layer solutions, neglecting entropy swallowing (a reasonable assumption for hemispheres), were performed for flow over hemispheres with $2.5 \le M_\infty \le 20$ and constant wall temperatures in the range $0.05 \le T_w/T_{0_\infty} \le 1.0$. The gas was treated as thermally and calorically perfect air, with $T_\infty = 200$ °R for $M_\infty = 2.5 \to 4$ and $T_\infty = 100$ °R for $M_\infty > 4$. The boundary-layer solutions were performed using the methods described in Ref. 5. The parameter $X$ was computed at the sonic point for each case.

Mayne assumed for a hemisphere that $T_e = C_1 T_{0_\infty}$, and using the similarity relationships

$$\frac{\theta}{r_n} \approx \frac{C_2}{\sqrt{Re_{\infty,r_n}}} \quad \text{and} \quad Re_{e,r_n} = C_3 Re_{\infty,r_n}$$

where $C_1, C_2$, and $C_3$ are constants. These substitutions permit the PANT correlation to be expressed in terms of a correlation similarity parameter $X$, trip height to local radius ratio $(k/r_n)$, and freestream Reynolds number based on nose radius. Local boundary-layer conditions such as $Re_{e,\theta}, T_e$, and $T_w$ are contained in the parameter $X$. Thus the PANT formula became

$$\lambda^* = X\left(\frac{k}{r_n}\right)^{0.7} (Re_{\infty,r_n})^{0.85} = 255 \text{ for effective tripping on the nosetip} \qquad (2)$$

where

$$X = Re^*_{e,\theta}\left[\frac{T^*_e}{T_w}\frac{r_n}{\theta^*}\right]^{0.7} \frac{1}{(Re_{\infty,r_n})^{0.85}} \qquad (3)$$

The * indicates conditions evaluated at the sonic point. Figure A1 (Appendix A) presents $X$ as a function of $T_w/T_{0_\infty}$ with $M_\infty$ as a parameter.

It should be noted that the PANT correlation and Mayne's reformulation of it are meant to predict transition on the hemispherical section of a nosetip only. It does not account for any "laminarization" that might occur as a result of the expansion around the shoulder. When one attempts to use $\lambda^*$ as a correlating parameter for distributed roughness on blunt-slender cones (see Fig. 4), the results are not satisfactory. One notes, for instance, a strong dependence on Mach number for which $\lambda^*$ fails to account. This is most likely caused by the expansion process that, of course, is a strong function of $M_\infty$ and cone angle. If a $\lambda^*_{\text{critical}}$ is defined as that $\lambda^*$ required to bring the end of transition $s_t$ up to a point near the trip, from Fig. 4 one can crossplot $\lambda^*_{\text{critical}}$ vs $M_\infty$ as shown in Fig. 5a. A definite correlation with Mach number is noted. Cone angle also has an effect on $\lambda^*_{\text{critical}}$ as noted in Fig. 5b. The Mach number and cone angle dependence of $\lambda^*$ clearly points to a requirement of adding (to the PANT correlation) a term that characterizes the expansion process when the correlation is to be applied to the conical section of a body. This term must account for variations in the strength of the expansion attributable to changes in Mach number and cone angle.

Analysis indicated that the ratio of local static pressure at the end of the gritted area $P_E$ to the pitot pressure $P'_0$ would effectively characterize the expansion. Hence, $P_E/P'_0$ alone accounts for both Mach number and cone angle variations.

Hence, a modified $\lambda^*$ may be defined as

$$\lambda^*_M = (X) f\left(\frac{k}{r_n}, Re_{\infty,r_n}, \frac{P_E}{P'_0}\right) \qquad (4)$$

One would expect, of course, that the relationships among the various terms of Eq. (4) would differ from the PANT formulation since the equation is being applied to a physically and aerodynamically different part of the body. The PANT formulation and Mayne's reformulation are valuable, however, in that they identify the significant variables.

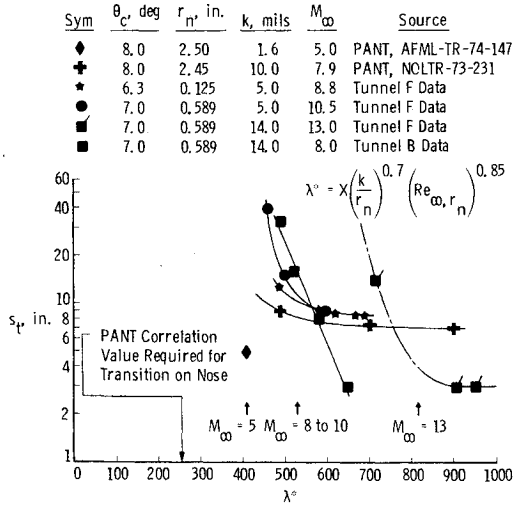


**Fig. 4 Correlation of distributed-roughness tripping results with PANT parameter λ*.**

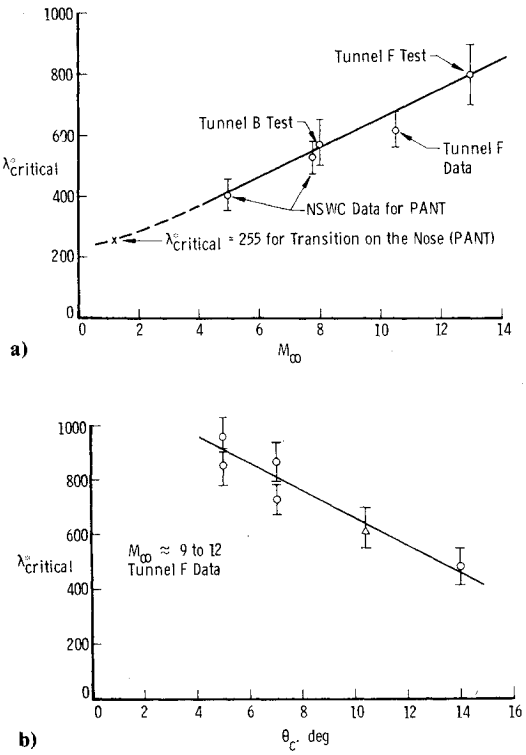


**Fig. 5 Effects of Mach number and cone angle on $\lambda^*_{\text{critical}}$. a) Mach number effects on $\lambda^*_{\text{critical}}$. b) Variation of $\lambda^*_{\text{critical}}$ with cone angle.**

Applying an analysis of these variables to the previous data[1] and the present results, a correlation was derived as shown in Fig. 6. As one may note from the limits listed in the figure, a fairly wide range of variables has been correlated. Special notes should be taken of the limits on $k/r_n$. Obviously one could choose a combination of variables outside these limits (i.e., low $Re_\infty$/ft, $r_n$, and $\theta_c$) that would yield unrealistic values of $k/r_n$. Within the stated limits, however, the correlation appears quite good.

The combination of cold-wall models and hypersonic wind tunnels operating at saturation temperatures yielded an essentially constant value of $X (X \approx 0.3)$. Hence, the new

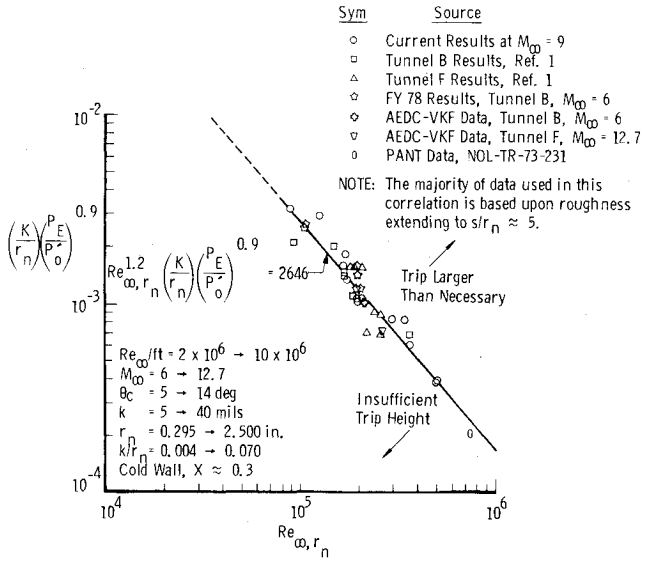


**Fig. 6 Distributed-roughness tripping correlation.**

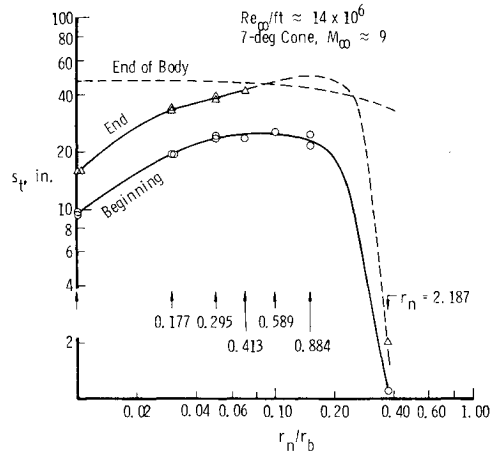


**Fig. 7 Blunt cone natural transition at $Re_\infty/ft \approx 14 \times 10^6$.**

correlation becomes

$$\lambda_M^* = X\left(\frac{k}{r_n}\right)\left(\frac{P_E}{P_0'}\right)^{0.9}(Re_{\infty,r_n})^{1.2} \tag{5}$$

and

$$\lambda^*_{M_{\text{critical}}} \approx 800 \tag{6}$$

for transition immediately behind the trip location. Therefore, for effective tripping with distributed-roughness-type trips, $\lambda_M^* \geq 800$. One should note that the roughened area should extend approximately from 45 deg off the stagnation point to $s/r_n = 5$, as pointed out in the previous work.[1] The $s/r_n = 5$ criterion for the termination of roughness appears to be adequate in terms of overcoming the expansion process and at the same time practical in terms of the amount of area roughened. Its use is highly recommended by the author.

One may solve Eq. (5) for $k$ by obtaining an appropriate value of $X$ from Fig. A1 of Appendix A and likewise a value of $P_E/P_0'$ from Fig. A2 (where $P_E/P_0'$ is evaluated at $s/r_n = 5$). Values of $k$ are correlated with standard grit number in Fig. A3.

It has been widely observed that trip effectiveness is somewhat related to the natural (untripped) transition location. The natural transition location in turn is a function of the nose radius as observed by Stetson and Rushton.[6] Therefore, one would want a correlation for tripping to be applicable at the worst condition, i.e., the nose radius that produces the greatest rearward displacement of natural transition location. Figure 7 shows that this is indeed the case for the correlation presented herein. Data[7] from the 7 deg cone (Fig. 1) indicate that the maximum rearward displacement of the beginning of transition occurs between $r_n = 0.259$ and 0.884 in., which is the range of most data used in Fig. 6. It should be noted that the majority of data correlated in Fig. 6 are for $r_n = 0.500 \rightarrow 0.589$ in. only four data points fall outside that range.

Since this correlation was developed solely from ground test data, additional work will be required to verify its use for flight vehicles. Factors such as ablation are known to affect natural transition and are likely to affect induced transition as well.

## Conclusions

1) The unmodified PANT formula fails to correlate roughness-induced transition on the conical sections of blunt-slender cones.

2) Both Mach number and cone angle effects must be accounted for in an adequate correlation parameter.

3) The inviscid pressure ratio $P_E/P_0'$ at $s/r_n = 5$ adequately models the expansion process (hence the Mach number and cone angle effects) on blunt cones.

4) Blunt cone roughness-induced transition data can be correlated using a modified version of the PANT correlation [Eqs. (5) and (6)].

5) Roughness should extend from $s/r_n = 0.8$ to 5 for adequate tripping.

6) The present correlation represents the range of nose radii that are most difficult to trip.

## Appendix A: Plots for Use with the λ*Correlation

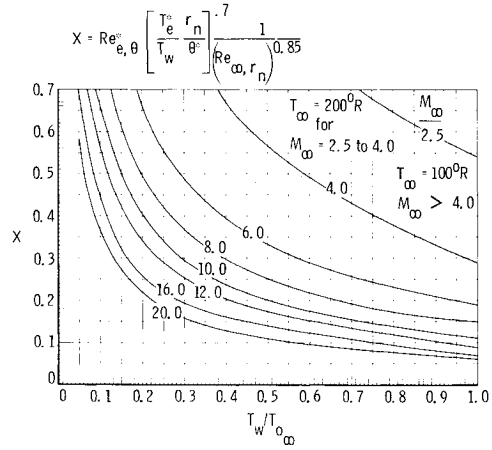


**Fig. A1 Correlation similarity parameter for thermally and calorically perfect air.**

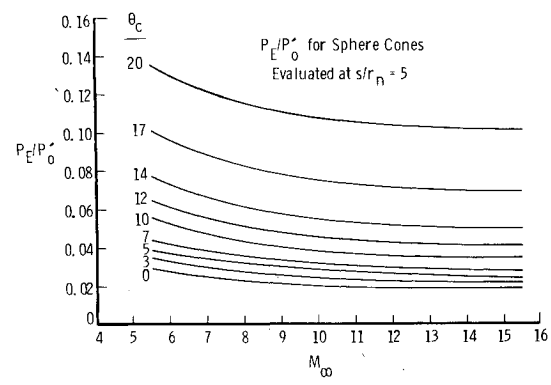


**Fig. A2 Inviscid three-dimensional characteristics pressure ratio for $s/r_n = 5$.**

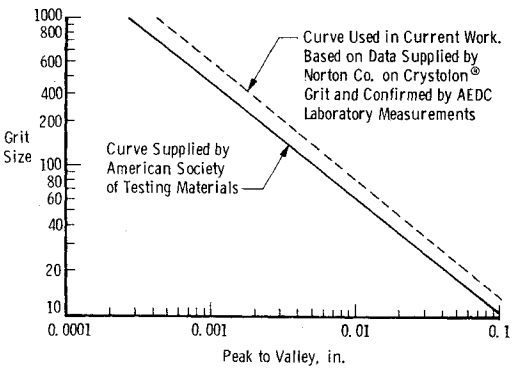


**Fig. A3 Values of $k$ correlated with standard grit number.**

## Appendix B: Tabulated Results

**Table B1 Primary variables and test results**

| Model | Data Group | $M_\infty$ | $Re_\infty$/ft x $10^{-6}$ | $r_{n'}$ in. | k, in. | Type Trip[2] | Extent of $s/r_n$ Range | $s_t$[1] in. |
|---|---|---|---|---|---|---|---|---|
| 5-deg | 6020 | 8.3 | 10.1 | 0.5 | 0.014 | Distributed Grit | 0.8 - 5.0 | 5 |
| | | 8.3 | 8.2 | | | | | 5 |
| | | 8.5 | 5.0 | | | | | 5 |
| | | 8.5 | 4.0 | | | | | 7 |
| | | 8.6 | 3.0 | | | | | 10 |
| | | 8.7 | 2.5 | | | | | 22 |
| | | 8.7 | 2.0 | | | | | 30 |
| 5-deg | 6021 | 8.2 | 10.0 | 0.5 | 0.020 | Distributed Grit | 0.8 - 5.0 | 5 |
| | | 8.3 | 8.1 | | | | | 5 |
| | | 8.4 | 5.0 | | | | | 5 |
| | | 8.5 | 4.1 | | | | | 5 |
| | | 8.9 | 3.0 | | | | | 10 |
| | | 9.2 | 2.5 | | | | | 28 |
| | | 9.3 | 2.0 | | | | | Transition |
| | | 9.4 | 1.5 | | | | | Laminar |
| 5-deg | 6022 | 8.1 | 10.5 | 0.5 | 0.036 | Distributed Grit | 0.8 - 5.0 | 5 |
| | | 8.2 | 8.2 | | | | | 5 |
| | | 8.3 | 5.3 | | | | | 5 |
| | | 8.4 | 4.1 | | | | | 5 |
| | | 8.6 | 3.0 | | | | | 5 |
| | | 9.0 | 2.5 | | | | | 30 |
| | | 9.2 | 2.0 | | | | | Transition |
| | | 9.2 | 1.7 | | | | | |
| 5-deg | 6023 | 8.9 | 18.2 | 0.5 | 0.010 | Distributed Grit | 0.8 - 5.0 | 5 |
| | | 8.8 | 14.3 | | | | | 5 |
| | | 8.6 | 10.2 | | | | | 5 |
| | | 8.4 | 8.2 | | | | | 8 |
| | | 8.2 | 6.0 | | | | | 25 |
| | | 8.1 | 5.1 | | | | | Transition |
| 5-deg | 6024 | 8.1 | 10.3 | 0.5 | 0.010 | Distributed Grit | 0.8 - 5.0 | 5 |
| | | 8.4 | 7.1 | | | | | 5 |
| | | 8.5 | 5.2 | | | | | 7 |
| | | 8.6 | 4.1 | | | | | 10 |
| | | 8.7 | 3.5 | | | | | 28 |
| | | 8.9 | 3.0 | | | | | Transition |
| | | 9.0 | 2.5 | | | | | Laminar |
| | | 9.0 | 2.3 | | | | | Laminar |
| 7-deg | 6005 | 9.0 | 20.3 | 0.589 | No | Trips | --- | 33 |
| | | 9.1 | 17.9 | | | | | 41 |
| | | 9.0 | 13.9 | | | | | 44 |
| | | 8.8 | 10.1 | | | | | Transition |
| | | 8.7 | 8.1 | | | | | |
| | | 8.6 | 6.3 | | | | | |
| 7-deg | 6006 | 8.9 | 20.5 | 0.589 | 0.005 | Grit Blasted | 0.0 - 5.0 | 4 |
| | | 9.1 | 18.1 | | | | | 4 |
| | | 9.0 | 14.0 | | | | | 4 |
| | | 8.8 | 10.0 | | | | | 4 |
| | | 8.8 | 8.0 | | | | | 44 |
| | | 8.7 | 6.0 | | | | | Transition |
| 7-deg | 6007 | 8.4 | 5.1 | 0.589 | 0.014 | Distributed Grit | 0.8 - 5.0 | 4 |
| | | 8.3 | 4.0 | | | | | 4 |
| | | 8.3 | 3.1 | | | | | 6 |
| | | 8.4 | 2.5 | | | | | 30 |
| | | 8.3 | 2.0 | | | | | 31 |
| | | 8.5 | 1.8 | | | | | Transition |
| 7-deg | 6008 | 8.7 | 4.5 | 0.589 | 0.014 | NCM | 0.10 - 5.0 | 4 |
| | | 8.8 | 4.0 | | | | | 4 |
| | | 9.0 | 3.5 | | | | | 31 |
| | | 8.8 | 2.5 | | | | | 40 |
| | | 8.7 | 2.0 | | | | | Transition |
| | | 8.7 | 1.7 | | | | | Laminar |
| 7-deg | 6009 | 8.0 | 3.1 | 0.589 | 0.040 | Distributed Grit | 0.8 - 5.0 | 4 |
| | | 8.0 | 2.6 | | | | | 4 |
| | | 8.3 | 2.0 | | | | | 4 |
| | | 8.3 | 1.6 | | | | | 6 |
| | | 8.4 | 1.0 | | | | | 31 |
| | | 8.6 | 0.8 | | | | | Transition |
| | | 8.5 | 0.5 | | | | | Laminar |
| 7-deg | 6010 | 8.2 | 10.3 | 0.589 | 0.005 | Distributed Grit | 0.0 - 5.0 | 4 |
| | | 8.7 | 8.2 | | | | | 5 |
| | | 8.2 | 5.2 | | | | | 8 |
| | | 8.1 | 4.0 | | | | | 14 |
| | | 8.1 | 3.0 | | | | | 44 |
| | | 8.3 | 2.6 | | | | | Transition |
| | | 8.5 | 2.0 | | | | | Laminar |
| | | 8.6 | 1.5 | | | | | |
| | | 8.8 | 1.1 | | | | | |

**Table B1 (con't.)**

| Model | Data Group | $M_\infty$ | $Re_\infty$/ft x $10^{-6}$ | $r_{n'}$ in. | k, in. | Type Trip[2] | Extent of $s/r_n$ Range | $s_t$[1] in. |
|---|---|---|---|---|---|---|---|---|
| 7-deg | 6011 | 8.4 | 5.9 | 0.589 | 0.063 & 0.109 | Spheres | 3.1 & 6.5 | 4 |
| | | 8.6 | 4.0 | | | | | 4 |
| | | 8.9 | 3.7 | | | | | 30 |
| | | 9.0 | 3.6 | | | | | 31 |
| | | 9.3 | 4.0 | | | | | 31 |
| | | 9.3 | 3.7 | | | | | 32 |
| | | 9.3 | 3.0 | | | | | 32 |
| | | 9.2 | 2.5 | | | | | 34 |
| | | 8.8 | 1.9 | | | | | Transition |
| 7-deg | 6012 | 8.5 | 8.0 | 0.589 | 0.063 & 0.109 | Spheres | 3.1 & 6.5 | 4 |
| | | 8.2 | 5.1 | | | | | 4 |
| | | 8.3 | 4.0 | | | | | 4 |
| | | 8.7 | 3.0 | | | | | 30 |
| | | 9.1 | 2.0 | | | | | 32 |
| 7-deg | 6013 | 8.5 | 10.0 | 0.589 | 0.008 | NCM | 0.10 - 5.0 | 4 |
| | | 8.7 | 7.5 | | | | | 6 |
| | | 8.4 | 5.1 | | | | | 29 |
| | | 8.5 | 4.0 | | | | | 33 |
| | | 8.8 | 3.5 | | | | | 35 |
| | | 9.1 | 3.0 | | | | | 44 |
| | | 8.6 | 2.5 | | | | | Transition |
| Biconic | 6016 | 8.9 | 20.8 | 0.589 | No | Trips | --- | 30 |
| | | 8.9 | 18.6 | | | | | 30 |
| | | 9.1 | 14.3 | | | | | 30 |
| | | 8.8 | 10.2 | | | | | 30 |
| | | 8.6 | 8.1 | | | | | Transition |
| | | 8.6 | 7.6 | | | | | Transition |
| Biconic | 6017 | 8.2 | 5.2 | 0.589 | 0.014 | Distributed Grit | 0.8 - 5.0 | 3 |
| | | 8.4 | 4.0 | | | | | 3 |
| | | 8.6 | 3.5 | | | | | 3 |
| | | 8.8 | 3.0 | | | | | 14 |
| | | 8.6 | 2.8 | | | | | Transition |
| | | 8.7 | 2.5 | | | | | |
| | | 8.4 | 2.0 | | | | | |
| Biconic | 6018 | 8.3 | 5.1 | 0.589 | 0.039 | Spherical | 6.8 | 5 |
| | | 8.4 | 4.0 | | | | | 8 |
| | | 9.1 | 3.1 | | | | | 14 |
| | | 9.3 | 2.5 | | | | | 14 |
| | | 9.4 | 2.0 | | | | | 14 |
| | | 9.3 | 1.7 | | | | | Transition |
| Biconic | 6019 | 8.3 | 10.3 | 0.589 | 0.010 | Distributed Grit | 0.8 - 5.0 | 3 |
| | | 8.4 | 7.5 | | | | | 3 |
| | | 8.3 | 5.1 | | | | | 3 |
| | | 8.3 | 4.0 | | | | | 3 |
| | | 8.5 | 3.5 | | | | | 3 |
| | | 9.0 | 3.1 | | | | | 14 |
| | | 8.8 | 2.5 | | | | | 14 |
| | | 8.6 | 2.3 | | | | | 14 |

## Acknowledgments

The work reported herein was conducted by the Arnold Engineering Development Center (AEDC), Air Force Systems Command (AFSC). The results presented herein were obtained by personnel of ARO, Inc., a Sverdrup Corporation company, operating contractor of AEDC. The tests were sponsored by AEDC/DOT. Further reproduction is authorized to satisfy needs of the U.S. Government.

## References

[1] Boudreau, A.H., "Artificially Induced Boundary-Layer Transition on Blunt-Slender Cones at Hypersonic Speeds," *Journal of Spacecraft and Rockets*, Vol. 16, July-Aug. 1979, pp. 245-251.

[2] "von Kármán Gas Dynamics Facility," Vol. 3, *Test Facilities Handbook* (11th Ed.), Arnold Engineering Development Center, June 1979.

[3] Pate, S.R. and Eaves, R.H., Jr., "Recent Advances in the Performance and Testing Capabilities of the AEDC-VKF Tunnel F (Hotshot) Hypersonic Facility," Paper 74-84 presented at AIAA 12th Aerospace Sciences Meeting, Washington, D.C., Jan. 30-Feb. 1, 1974.

[4] Anderson, A.D., "Boundary-Layer Transition on Nosetips with Rough Surfaces," Appendix, Vol. X, *Interim Report Passive Nosetip Technology (PANT) Program*, Vols. I-XV, SAMSO-TR-74-86 (AD-A020708), Jan. 1975.

[5] Mayne, A.W., Jr. and Dyer, D.F., "Comparison of Theory and Experiment for Turbulent Boundary Layers on Simple Shapes at Hypersonic Conditions," *Proceedings of the 1970 Heat-Transfer and Fluid Mechanics Institute*, Stanford University Press, Stanford, Calif., 1970, pp. 168-188.

[6] Stetson, K.F. and Rushton, G.H., "Shock Tunnel Investigation of Boundary-Layer Transition at $M=5.5$," *AIAA Journal*, Vol. 5, May 1967.

[7] Stetson, K.F., "Effect of Bluntness and Angle-of-Attack on Boundary-Layer Transition on Cones and Biconic Configurations," Paper 79-0269 presented at AIAA 17th Aerospace Sciences Meeting, New Orleans, La., Jan. 15-17, 1979.